Journal of Power Sources 195 (2010) 3309–3315

Contents lists available at ScienceDirect

Journal of Power Sources

journal homepage: www.elsevier.com/locate/jpowsour

Electrochemical recovery of cobalt and copper from spent Li-ion batteries as multilayer deposits

M.B.J.G. Freitas*, V.G. Celante, M.K. Pietre

Universidade Federal do Espírito Santo, Departamento de Química, Laboratório de Eletroquímica Aplicada, Av. Fernando Ferrari 514, Goiabeiras, Vitória-ES, CEP: 29070-910, Brazil

ARTICLE INFO

Article history:
Received 31 October 2009
Received in revised form
22 November 2009
Accepted 25 November 2009
Available online 2 December 2009

Keywords:
Li-ion batteries
Cobalt
Copper
Recycling
Electrodeposition

ABSTRACT

In this work, spent Li-ion batteries were used to form cobalt and copper multilayers by electrodeposition. The effects of pH on the nucleation and growth mechanism, morphology and crystalline structure were studied. The instantaneous nucleation mechanism occurs at pH 2.7 and progresses at pH 5.4 for cobalt electrodeposition on platinum, vitreous carbon and aluminum. Copper can be electrodeposited on cobalt by an instantaneous mechanism at pH 2.7 and progressively at pH 5.4. Using scanning electron microscopy, we verified a more porous electrodeposit at pH 5.4 than at pH 2.7. X-ray diffractograms showed the peaks of Cu_2O, CuO and the Co and Cu cubic centered face structures for both pH values at a charge density of 2.00 and 10.0 C cm^{-2}. The electric circuit obtained by electrochemical impedance spectroscopy for Co–Cu multilayer growth at both pH 2.7 and 5.4 with a charge density equal to 2.0 and 10.0 C cm^{-2} on Al has the form $R_s(R_pQL)$. The presence of the constant phase element (Q) is attributed to the irregularity of the Co–Cu multilayer electrodeposits, and the inductive element (L) is associated with cobalt dissolution in acidic solution.

1. Introduction

The cathode is the main component that determines the cost and the charge efficiency of Li-ion batteries. The cathode material is a composite of $LiMO_2$, where M is a transition metal. The oxides used as cathodic materials include cobalt ($LiCoO_2$), nickel ($LiNiO_2$), manganese ($LiMn_2O_4$) and vanadium (LiV_2O_3). The most commonly used material in cathodes is $LiCoO_2$. Nowadays, carbon materials with or without graphite are largely used as the anode material in Li-ion batteries, with PVDF as an agglomerate agent. The active material is pressed about a copper substrate. The copper substrate has a thickness of 14 μm and a length of 0.21 m. The separators are formed by a multilayer structure of polyethylene and polypropylene, forming a polymeric microporous membrane. The battery electrolyte composition is a mixture of ethylene carbonate (necessary for the passivity of the negative electrode), ethyl, dimethyl, diethyl and methyl-ethyl carbonates (EC, DMC, DEC and MEC, respectively) and $LiPF_6$ as the electrolytic solution [1,2].

The world production of Li-ion batteries reached 500 million units in 2000 and may surpass 4.6 billion in 2010 [2]. The use of portable devices such as cellular telephones and microcomputers has contributed to increased consumption.

The placement of spent Li-ion batteries in domestic garbage is becoming a serious environmental problem. One solution to the problem is battery recycling by pyrometallurgical or hydrometallurgical processes. A pyrometallurgical process is not desirable due to the emission of toxic gases into the environment. A hydrometallurgical process is thus more favorable from an environmental conservation viewpoint. In the hydrometallurgical process, after battery dismantling occurs, the electrodes are dissolved in concentrated acids. After this stage, the resultant solution, which contains metal ions, can be recovered by one of the three methods: precipitation, extraction or electrodeposition. Electrodeposition is a viable process to produce cobalt metallic films, alloys and multilayer deposits with controlled structure and morphology. The formation of a Co and Cu multilayer deposit is being widely studied due to its giant magneto resistance (GMR) [3]. The nucleation mechanism depends strongly on the bath composition and pH of the electrolyte [4,5]. Different nucleation processes, namely instantaneous or progressive, with 2D or 3D growth, are found in different electrolytes [6–9]. However, these studies are related to systems where only Co^{2+} or Cu^{2+} ions are present in the electrolyte. The objective of this work is to analyze the influence of the pH of the solution on the electrodeposition mechanism, morphology and crystalline structure of cobalt and copper multilayer electrodeposits. The Scharifker and Hills nucleation model was studied by applying a potentiostatic step technique in the initial stage of cobalt and copper electrodeposition. For multilayer characterization, scanning electronic microscopy (SEM), X-ray diffractometry (XRD), energy dispersive

* Corresponding author. Tel.: +55 27 33352486; fax: +55 27 33352460.
E-mail address: marcosbj@hotmail.com (M.B.J.G. Freitas).

0378-7753/$ – see front matter © 2009 Elsevier B.V. All rights reserved.
doi:10.1016/j.jpowsour.2009.11.131

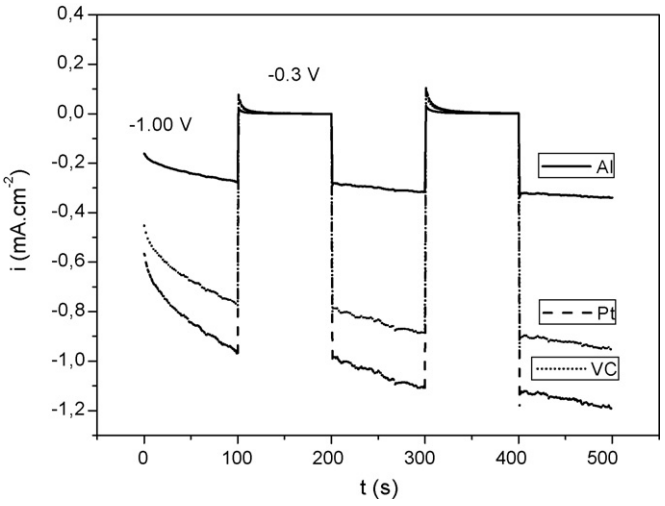

Fig. 1. Chronoamperograms of the Co and Cu system at pH 2.7, Al (–), Pt (—) and VC (···).

scanning (EDS), and electrochemical impedance spectroscopy (EIS) were used.

2. Experimental

2.1. Preparation of the electrodeposition solutions

The Co–Cu electrodeposition baths were formed with materials recovered from spent Li-ion batteries. Spent Li-ion batteries were physically dismantled and separated into their different parts: anode, cathode, organic separators, steel compartment and current collectors. The negative electrode (copper and carbon material) was separated. This material was dried at 120 °C for 24 h to evaporate the organic compounds present in the electrolyte solution, such as ethylene carbonate (EC) and propylene carbonate (PC). The current collector was also separated from the active material. The copper current collector was then washed with distilled water at 40 °C to eliminate lithium salts present in the electrolyte. A mass of 9.21 g of the current collector was dissolved in a solution containing 470.00 mL of 3.00 mol L^{-1} H_2SO_4 and 30.00 mL of 30% (v/v) H_2O_2, and the system was kept under magnetic stirring at 60 °C for 2 h. The addition of H_2O_2 is necessary to increase the efficiency of copper dissolution because copper is partially insoluble in H_2SO_4 solutions. The carbon active material was separated by filtration

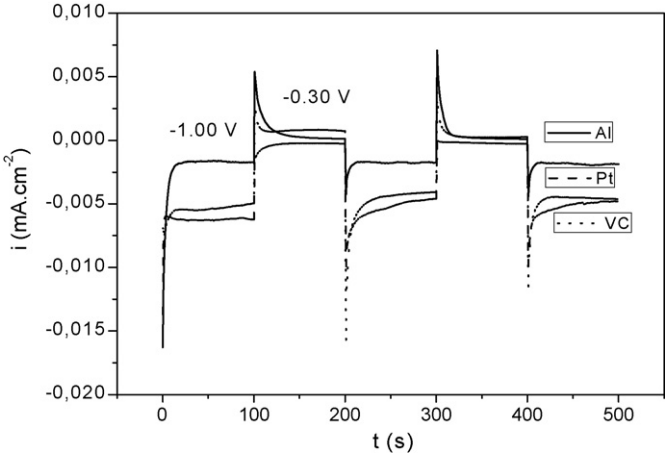

Fig. 2. Chronoamperograms of the Co and Cu system at pH 5.4, Al (–), Pt (—) and VC (···).

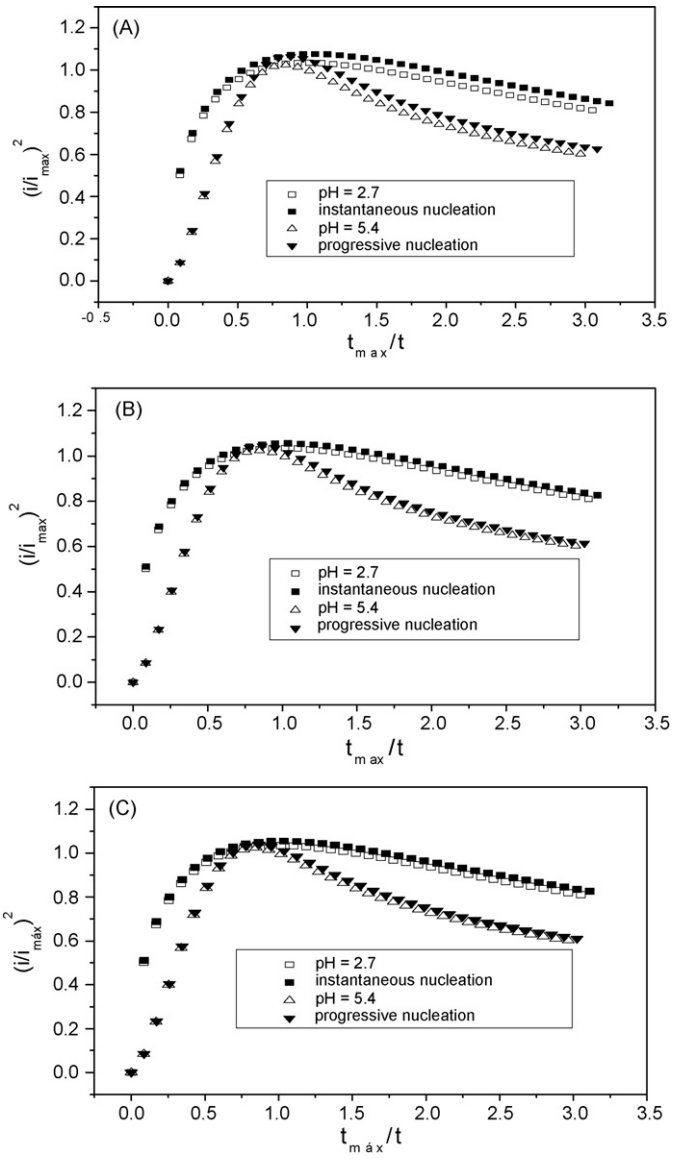

Fig. 3. Nucleation models for cobalt electrodeposits for Co–Cu multilayers in Al (A), Pt (B) and VC (C) substrates.

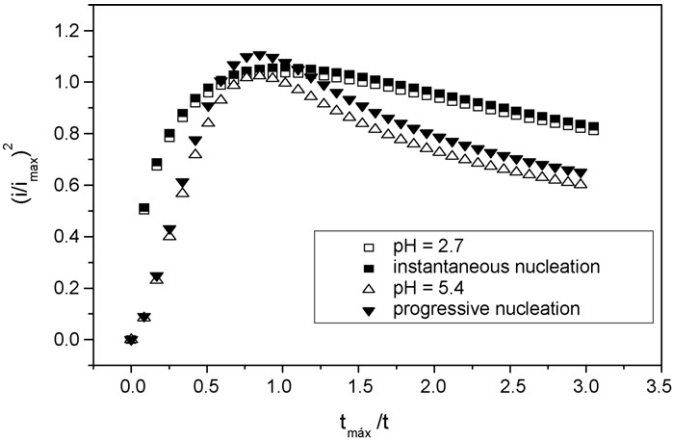

Fig. 4. Nucleation models for copper electrodeposits on Co substrates.

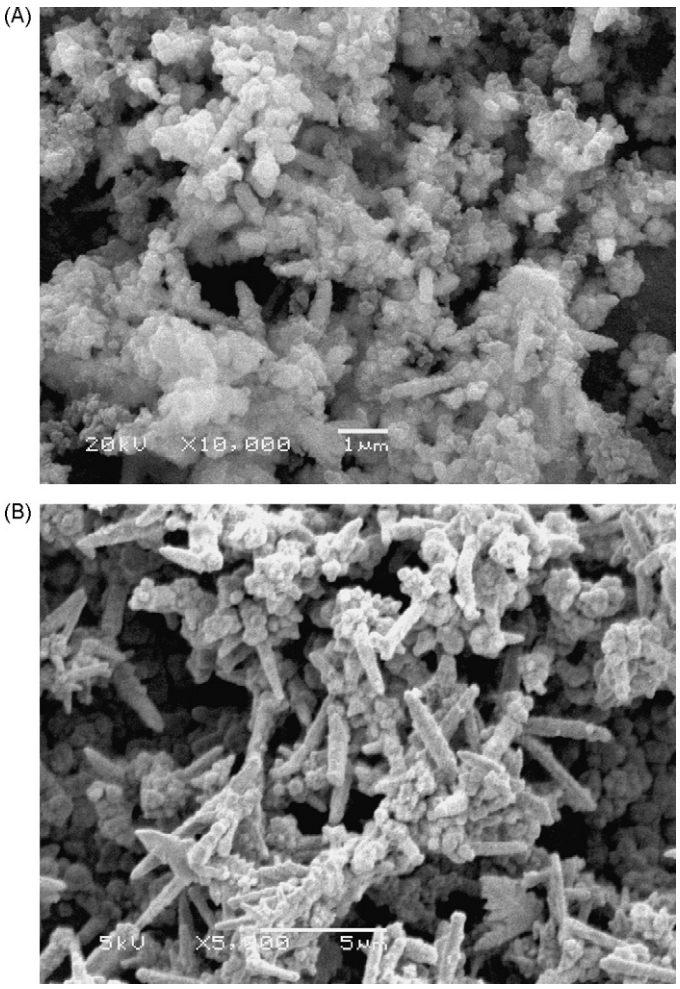

Fig. 5. SEM microphographs for Co–Cu multilayers, Al substrate, $q = 10.0\,C\,cm^{-2}$. (A) pH 2.7 and (B) pH 5.4.

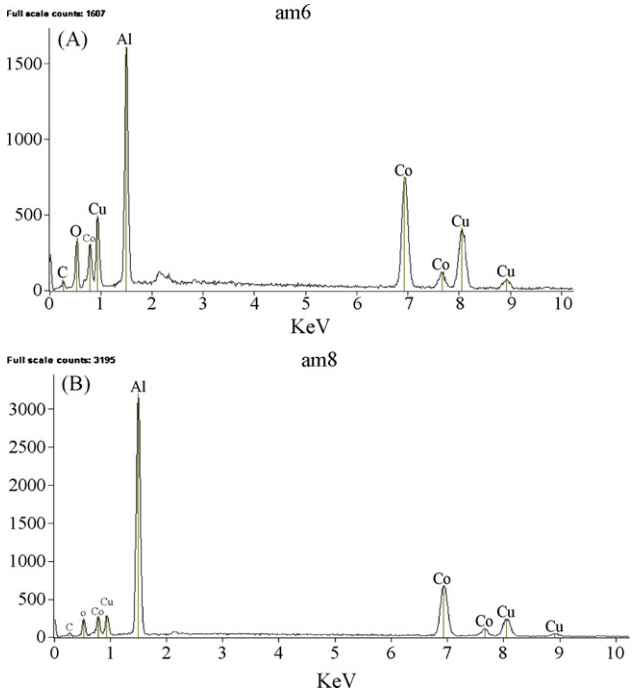

Fig. 6. Typical dispersive X-ray energy diagrams for the Co–Cu multilayer, Al substrate, $q = 10.0\,C\,cm^{-2}$. (A) pH 2.7 and (B) pH 5.4.

from the leaching solution. Eq. (1) describes the anode dissolution process:

$$Cu_{(s)} + H_2SO_{4(aq)} + H_2O_{2(liq)} \rightarrow CuSO_{4(aq)} + 2H_2O_{(liq)} \quad (1)$$

For cobalt dissolution, a mass of 9.17 g of positive electrodes was dissolved in a solution containing 470.00 mL of 3.00 mol L^{-1} H_2SO_4 and 30.00 mL of 30% (v/v) H_2O_2. The system was maintained under constant magnetic agitation at 80 °C for 2 h. The insoluble carbon black was separated by filtration from the leaching solution. The addition of H_2O_2 is necessary to increase the efficiency of cathode dissolution. H_2O_2 reduces cobalt from an oxidation state of III+, which is insoluble in aqueous systems, to an oxidation state of II+, which is soluble in water. Considering the active material $LiCoO_2$, the cathode dissolution reaction is represented by Eq. (2) below:

$$2LiCoO_{(s)} + H_2O_{2(liq)} + 3H_2SO_{4(aq)} \rightarrow 2CoSO_{4(aq)} + Li_2SO_{4(aq)} + 4H_2O_{(liq)} + O_{2(g)} \quad (2)$$

The pH of the leaching solution was adjusted with NaOH pellets to 2.7 and 5.40. The solutions were buffered with 0.10 mol L^{-1} H_3BO_3. The function of the H_3BO_3 was to maintain the constant pH of the electrodeposition bath, because this influences the efficiency and morphology of the electrodeposits.

The ionic cobalt and copper concentrations in the baths were equal to 0.10 and 1.0×10^{-3} mol L^{-1} as measured by inductively coupled plasma mass spectroscopy (ICP-MS).

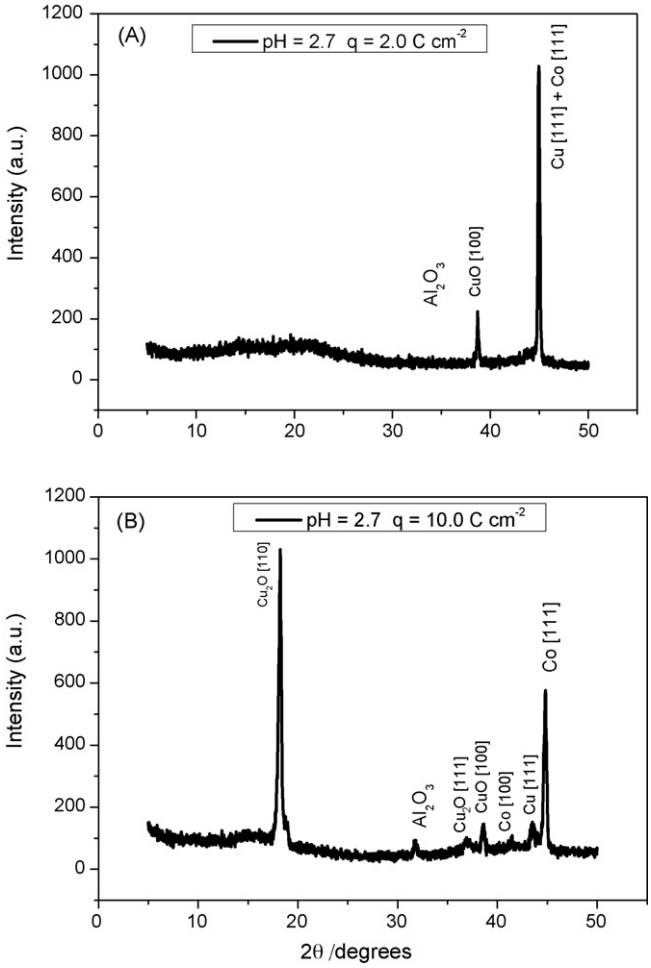

Fig. 7. Typical X-ray diffraction for Co–Cu multilayers, Al substrate, at pH 2.7. (A) $q = 2.0\,C\,cm^{-2}$ and (B) $q = 10.0\,C\,cm^{-2}$.

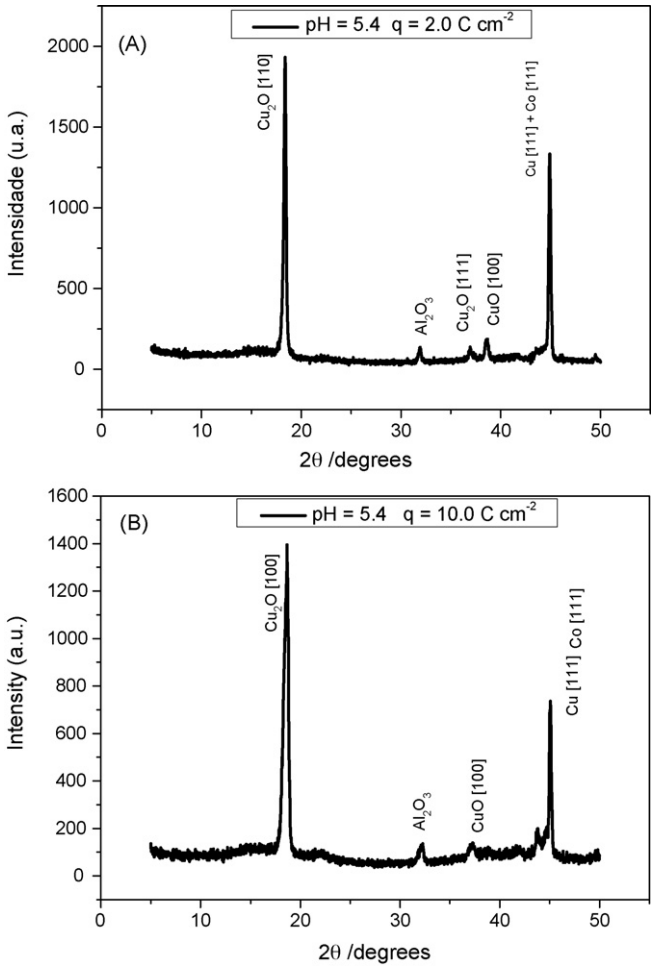

Fig. 8. Typical X-ray diffraction, Al substrate, at pH 5.4. (A) $q = 2.0\,C\,cm^{-2}$ and (B) $q = 10.0\,C\,cm^{-2}$.

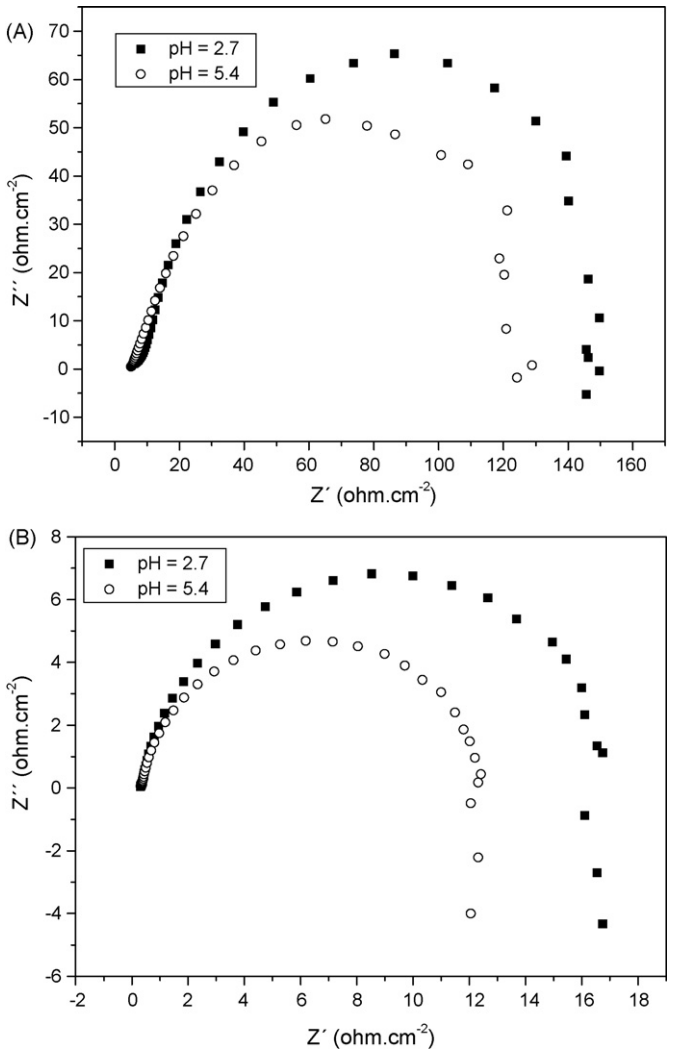

Fig. 9. Nyquist plot for Co–Cu multilayers, Al substrate, at both pH. (A) $q = 2.0\,C\,cm^{-2}$, (B) $q = 10.0\,C\,cm^{-2}$.

2.2. Electrochemical measurements

Potentiostatic experiments were performed in an AUTOLAB PGSTAT 100 with an electrochemical impedance spectroscopy (EIS) module. The working electrode was composed of Al (98%, MERCK, 0.25 cm^2), platinum and vitreous carbon. The counter electrode was composed of platinum (3.00 cm^2), and the reference electrode was saturated Ag/AgCl/KCl.

A Co and Cu multilayer electrodeposit was made in potentiostatic steps, which consisted of applying a cobalt deposition potential (−1.00 V) for a time interval (50 and 100 s) and then stepping directly to the copper deposition potential (−0.30 V). Under these conditions, the cobalt deposition charge efficiency is 98% [5]. The copper and cobalt potentials at concentrations of 1.0×10^{-3} and 1.0 10^{-1} mol L^{-1} are equal to 0.047 vs. Ag/AgCl and −0.511 V vs. Ag/AgCl, respectively. Therefore, the Cu eletrodeposition on the Co layer is a spontaneous reaction. For copper electrodeposition, a potential of −0.3 V was chosen. At this potential, the preferential deposition of ionic copper occurs, and the cobalt deposits do not oxidize during the copper deposition. The charge densities applied in this work were equal to 2.00 and 10.0 C cm^{-2}. The bilayer thickness (h_b) was calculated by Faraday's Law, as shown in Eq. (3) below:

$$l = \overline{nFA}\left[\frac{M_{Cu}Q_{Cu}}{\rho_{Cu}} + \frac{M_{Co}Q_{Co}}{\rho_{Co}}\right] \quad (3)$$

where Q_{Cu} and Q_{Co} are the charge density applied in copper and cobalt electrodeposition, and M_{Cu} and M_{Co} are the molar masses, equal to 63.3 and 56.3 g mol^{-1}, respectively; F is the Faraday's constant (96485 C mol^{-1}), and A is the electrode geometric area (0.25 cm^2). For 2.0 C cm^{-2}, the bilayer thickness was equal to 1230 μm, and at 10.0 C cm^{-2} it was equal to 6150 μm.

EIS was performed in an AUTOLAB PGSTAT 100 with an EIS module in the frequency range of 1.0 MHz to 0.1 mHz with an amplitude of 10 mV in 0.5 mol L^{-1} H_2SO_4. The open circuit potential was equal to −0.540 V for pH 2.7 and −0.553 V for pH 5.4. The data obtained were analyzed by the program FRA of AUTOLAB for the simulations of equivalent circuits. All the electrochemical experiments were performed at 25 °C.

Table 1
Percentage composition of the Co–Cu multilayer electrodeposit.

Element	pH = 5.4 composition (%)	pH = 2.7 composition (%)
Co	23.72	40.67
Cu	5.56	11.57
O	13.60	10.79
Al	32.52	19.38
C	24.60	17.38

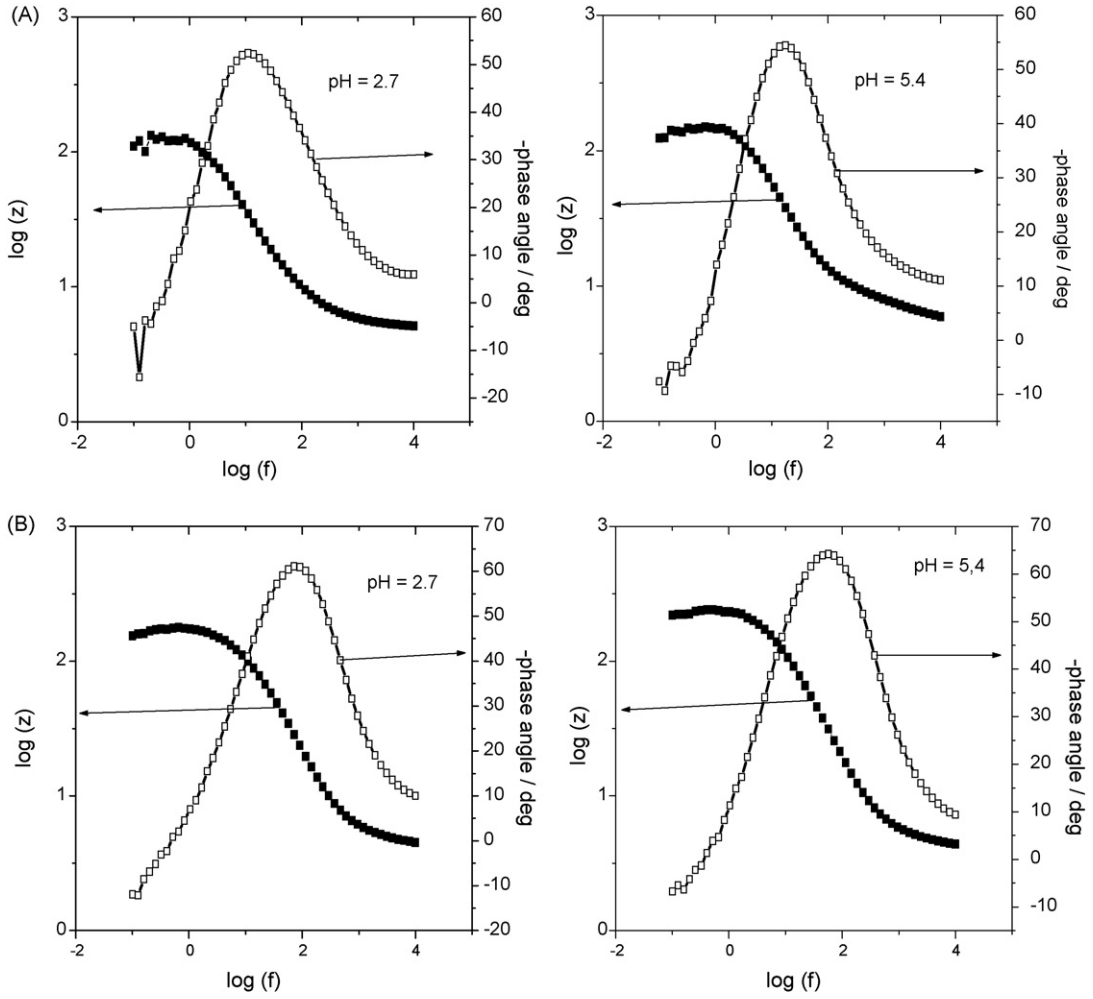

Fig. 10. Bode plot for Co–Cu multilayers, Al substrate, (A) $q = 2.0\,C\,cm^{-2}$, pH 2.7 and pH 5.4, (B) $q = 10.0\,C\,cm^{-2}$, pH 2.7 and pH 5.4.

2.3. Material characterization

DRX analysis was performed in a Shimadzu CRD 7000 diffractometer, at room temperature, with Cu Kα radiation, 40.0 kV, and 30.0 mA. The diffractograms were obtained in $2\Theta = 1.40–50.0^{\circ}$. X-ray measurements were performed with copper K_{α} radiation, a Ni filter, and scan speed of $2^{\circ}\,min^{-1}$. Inductively Coupled Plasma Mass Spectroscopy (ICP-MS) measurements were made with the aid of a Varian 715-ES. Scanning electron microscopy (SEM) and energy dispersive scanning (EDS) analysis were performed with a JEOL 6360LV microscope, with previous covering with carbon in a Bal-Tec MED020 vaporizer.

3. Results and discussion

3.1. Nucleation and growth of the cobalt and copper multilayer

Figs. 1 and 2 represent typical chronoamperograms of the Co and Cu system at pH 2.7 and 5.4 for 100 s of deposition for each element with Pt, vitreous carbon (VC) and aluminum substrates. The current density is smaller in the aluminum than in the Pt and VC electrodes due to the oxide film on the Al surface. The current density related to cobalt deposition at pH 2.7 is larger than at pH 5.4 during the whole electrodeposition process. This is related to the electrodeposition of cobalt simultaneous with the hydrogen detachment reaction. The cobalt electrodeposit nucleation and growth models on the Al, Pt and VC substrates are analyzed in Fig. 3A (Al), B (Pt) and C (VC). It is noted that at pH 2.7, the model tends towards an instantaneous growth, where the nuclei are formed quickly over the whole substrate. This nucleation is related to two-dimensional growth (2D), and the electrodeposit shows a more homogeneous morphology. At pH 5.4, the growth tends to be due to the progressive mechanism, where the nucleation rate is slow with a large number of active sites, related to three-dimensional growth (3D). The small variation present on the Al substrate is due to the layer of oxide.

Electrodeposit nucleation models were also applied for copper on a cobalt substrate (Fig. 4). At pH 2.7, the experimental result approaches the theoretical one for instantaneous nucleation, and at pH 5.4 it tends to model progressive nucleation. However, a deviation between the experimental and theoretical results occurs because the copper deposition is under a previously existing layer of porous cobalt.

3.2. Co and Cu multilayer deposit characterization

Morphologic analysis of the Co and Cu multilayer electrodeposited on the Al substrate was made by SEM and EDS techniques. Fig. 5 shows the microphotograph of the Co and Cu multilayer deposited with a charge density of equal to $10.0\,C\,cm^{-2}$ at pH 2.7 (Fig. 5A) and 5.4 (Fig. 5B). It is possible to observe two distinct regions: one formed with small microporosity and another with larger porosity. The Co and Cu multilayer electrodeposited at pH 5.4 presents major macroporosity due to the predominant progressive

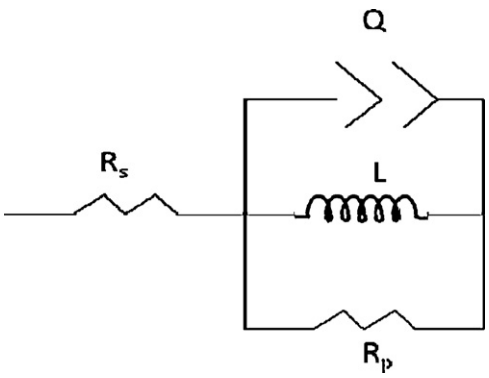

Fig. 11. Equivalent circuit for Co–Cu multilayers.

nucleation and three-dimensional growth. Fig. 6A shows typical dispersive X-ray energy diagrams for the Co–Cu multilayer at pH 2.7, and Fig. 6B shows data at pH 5.4.

The EDS measurements of the Co–Cu multilayer electrodeposits showed that the Co–Cu multilayer electrodeposit is made up of Co, Cu, Al, O and C. The quantitative composition of the surface is visualized in Table 1, where the percentage composition of the relative surface to the aluminum is observed. EDS analyses showed that the composition percentage of Al substrate is smaller at pH 2.7 than at pH 5.4. The composition percentage of Co and Cu is larger at pH 2.7 than at pH 5.4. This is in agreement with the proposal of the model of instantaneous nucleation at pH 2.7 with 2D growth, and progressive nucleation at pH 5.4 with 3D growth.

Fig. 7A is a typical X-ray diffractogram of a Co and Cu multilayer deposit formed by applying a charge density equal to 2.0 C cm^{-2} in solutions at pH 2.7. The presence of an Al_2O_3 layer on the aluminum substrate can be observed, [1 0 0] of CuO, Cu in the [1 1 1] direction and Co in the [1 1 1] direction [10–13]. With increasing charge density for q = 10.0 C cm^{-2} (Fig. 7B), the following peaks are observed: [1 1 0] for copper oxide, Cu_2O in the [1 1 1] direction [1 1 1], CuO in the [1 0 0] direction, cobalt in the [1 0 0] direction, and the face cubic centered structure of copper in the [1 1 1] direction and cobalt in the [1 1 1] direction [14,15]. In this case, the peaks referring to the face cubic centered structures of Co and Cu do not overlay a unique peak. According to the literature [16], the compact hexagonal structure is preferential for cobalt deposition. Cobalt tends to be stabilized in the cubic structure during electrodeposition in the presence of copper by potentiostatic stepping [9].

Fig. 8 is a typical X-ray diffractogram of a Co and Cu multilayer deposit formed by applying a charge density equal to 2.0 C cm^{-2} (Fig. 8A) and 10.0 C cm^{-2} (Fig. 8B) in solutions at pH 5.4. The following can be observed: the [1 1 0] direction of Cu_2O and Al_2O_3 from the aluminum substrate, specifically, [1 0 0] CuO, [1 0 0] CuO, [1 1 1] Cu and [1 1 1] Co.

3.3. Electrochemical impedance spectroscopy

The potentiodynamic, SEM, EDS and X-ray diffraction measurements were complemented by the electrochemical impedance spectroscopy (EIS) technique.

EIS consists of the study of interfaces and systems through the application of a senoidal electric potential with a variable frequency, which results in a senoidal current, and the phase angle, which consists of the change of the current in relation to the applied potential. This method of application of the potential allows for a disturbance in the system using only a few milivolts, making possible the investigation of phenomena in a close stationary state. In addition, it is possible to disturb the system using different frequency values because the potential wave is senoidal. If the disturbance in the system under investigation is of small width, it is possible to use the technique for the analysis of the stages of a reaction mechanism. Starting from these measurements, it is possible to study processes such as charge transport, conductivity of films, double layer capacity, diffusion transport, and charge reactions process, among others. The electrochemical system is modeled in agreement with an equivalent circuit of the form resistor/capacitor/inductor. In the Nyquist diagram, the resistance in the solution is represented by a resistance R_s at high frequencies, and $R_s + R_p$ at low frequencies. The capacitive elements in a circuit represent a delay between the current and the potential. The capacitance dispersions are represented by the constant phase element (CPE). The CPE is related to the irregular metallic electrodeposit. The presence of the inductive element (L) in the electrochemical system represents the advance of the current in relation to the potential. The inductive behavior is visualized in Nyquist diagrams as imaginary impedances below the x-axis in the fourth quadrant and in Bode diagrams as a positive variation of the phase angle.

In the systems that present effects of mass transfer, the introduction of an element denominated "Warburg impedance" is made with the purpose of simulating the characteristics of the experimental system in processes that suffer lineal, spherical diffusion or under forced convection. A semi-circle aspect is first observed in the Nyquist plot, followed by a straight line whose tangent to the real axis is 45°, as is characteristic of a Warburg diffusion process.

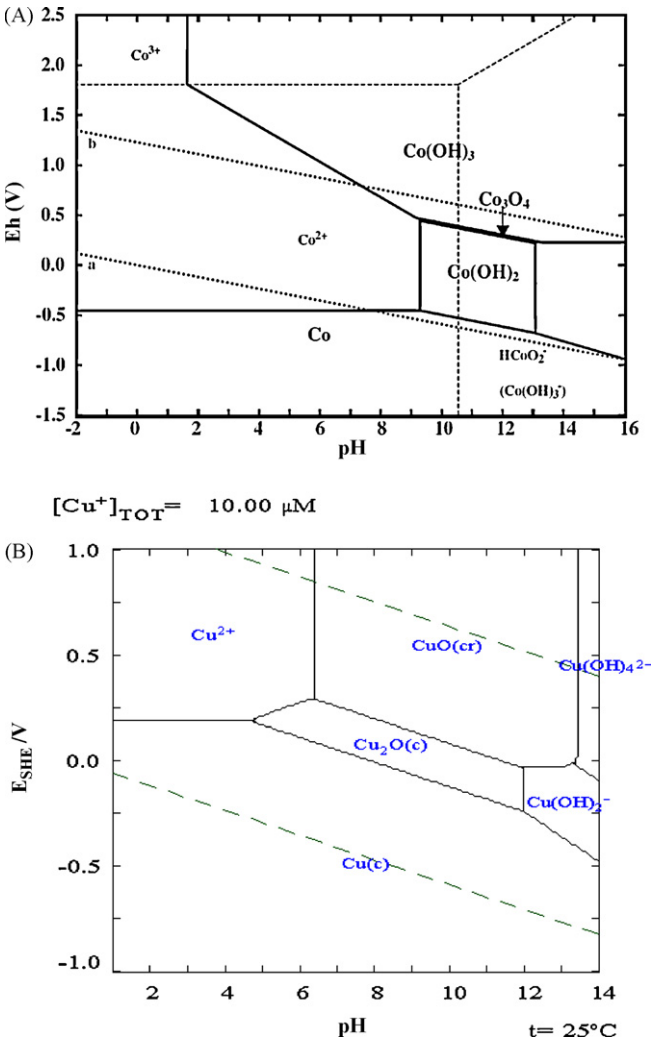

Fig. 12. Pourbaix diagram: (A) cobalt–H_2O system and (B) copper–H_2O system.

In this context, a group of factors can influence the impedance of the system, such as reaction and diffusion processes, and species adsorption. This provides EIS with a wide application field.

Fig. 9 represents a Nyquist diagram for Co and Cu multilayers grown at pH 2.7 and pH 5.4 with charge densities equal to 2.0 C cm^{-2} (Fig. 9A) and 10.0 C cm^{-2} (Fig. 9B) on an aluminum substrate. The Bode diagrams are visualized in Fig. 10A and B. The inductive behavior is visualized in the Nyquist diagrams as imaginary impedances below the *x*-axis in the fourth quadrant and in Bode diagrams as a positive variation of the phase angle. The equivalent circuit (Fig. 11) for both Co–Cu multilayer deposits was obtained with data treatment by FRA software. It was obtained in the form of a $R_s(R_pQL)$ circuit, where R_s is the solution resistance, R_p is the polarization resistance, L is an inductor, and Q is the constant phase element (CPE). The presence of the CPE element is due to the deviation of the ideal capacitor [17] due to the irregularity of the Co and Cu multilayer electrodeposits, as visualized in the microphotographs.

The presence of the inductive element (L) in the electrochemical system is associated with cobalt dissolution. The dissolution of metallic cobalt in the potential (−0.1 V vs. hydrogen electrode) and pH solutions (2.7 and 5.4) is a spontaneous reaction (as can be seen in Fig. 12A). Copper is in the passive state, as can be seen in the Pourbaix diagram in Fig. 12B.

4. Conclusion

The Scharifker and Hills nucleation models for cobalt electrodeposition on Al, Pt and VC substrates were studied. It was verified that at pH 2.7 the model tends to be instantaneous, and at pH 5.4 the model tends to be progressive. Nucleation models were applied to copper electrodeposited on cobalt. At pH 2.7, the experimental result approached the theoretical one for instantaneous nucleation, and at pH 5.4 it tended towards progressive nucleation. The morphologic analysis of the Co–Cu multilayer electrodeposited on the Al substrate was studied by SEM. The multilayer Co and Cu electrodeposited at pH 5.4 presented major porosity due to the predominant progressive nucleation mechanism observed in the electrodeposition of Co and Cu. The multilayer Co and Cu electrodeposited at pH 2.7 presented minor porosity due to the predominant instantaneous nucleation observed in the electrodeposition of Co and Cu.

The X-ray diffractograms of Co and Cu multilayer deposits at pH 2.7 with an applied charge density $q = 10.0$ C cm^{-2} and at pH 5.4 with an applied charge equal to 2.0 and 10.0 C cm^{-2} revealed the peaks for Cu_2O, CuO and the cubic face centered structure of cobalt and copper. The equivalent circuit obtained by the EIS technique for Co–Cu multilayers grown in both pH 2.7 and 5.4 solutions with charge densities equal to 2.0 and 10.0 C cm^{-2} on an aluminum substrate is described by $R_s(R_pQL)$. The presence of the CPE (Q) is attributed to the irregularity of the Co–Cu multilayer electrodeposit, and the inductive element (L) is associated with cobalt dissolution.

References

[1] N. Arai, T. Tanaka, K. Ohta, J. Power Sources 97/98 (2001) 2–6.
[2] K. Kanamura, W. Hoshikawa, T. Umegaki, J. Electrochem. Soc. 149 (2002) 339.
[3] M.N. Baibich, J.M. Broto, A. Fert, F. Nguyen Van Dau, F. Petroff, P. Etienne, G. Creuzet, A. Friederich, J. Chazelas, Phys. Rev. Lett. 61 (1988) 2472.
[4] J. Yahalom, O. Zadak, J. Mater. Sci. 22 (1987) 49.
[5] M.B.J.G. Freitas, E.M. Garcia, J. Power Sources 171 (2007) 953.
[6] M.B.J.G. Freitas, E.M. Garcia, V.G. Celante, J. Appl. Electrochem. 39 (2009) 601.
[7] E. Vallés, E. Gomez, A. Labarta, A. Llorente, Surf. Coat. Technol. 153 (2002) 261–266.
[8] L.F. Senna, F.L.G. Silva, J.R. Garcia, V.G.M. Cruz, A.S. Luna, D.C.B. Lago, J. Appl. Electrochem. 38 (2008) 1763–1769.
[9] D. Landolt, P. Bradley, Electrochim. Acta 45 (1999) 1077–1087.
[10] Joint Committee on Powder Diffraction Standards, Diffraction Data File, No. 54-019, JCPDS International Center for Diffraction Data, Pensylvania, 1991.
[11] Joint Committee on Powder Diffraction Standards, Diffraction Data File, No. 44-0706, JCPDS International Center for Diffraction Data, Pensylvania, 1991.
[12] Joint Committee on Powder Diffraction Standards, Diffraction Data File, No. 04-0836, JCPDS International Center for Diffraction Data, Pensylvania, 1991.
[13] Joint Committee on Powder Diffraction Standards, Diffraction Data File, No. 15-0806, JCPDS International Center for Diffraction Data, Pensylvania, 1991.
[14] Joint Committee on Powder Diffraction Standards, Diffraction Data File, No. 34-1354 JCPDS International Center for Diffraction Data, Pensylvania, 1991.
[15] Joint Committee on Powder Diffraction Standards, Diffraction Data File, No. 05-0727 JCPDS International Center for Diffraction Data, Pensylvania, 1991.
[16] K. Takeno, M. Ichimura, K. Takano, J. Yamaki, J. Power Sources 142 (2005) 298–305.
[17] A.J. Bard, L.R. Faulkner, Electrochemical Methods. Fundamentals and Applications, J. Wiley & Sons, New York, 2001, Chap. 1, 3, 4, 6 and 12.